21 AUG 1980

SECURITY CLASSIFICATION OF THIS PAGE (When Data Entered)

REPORT DOCUMENTATION PAGE	READ INSTRUCTIONS BEFORE COMPLETING FORM
1. REPORT NUMBER 7	2. GOVT ACCESSION NO. AD-A088 473	3. RECIPIENT'S CATALOG NUMBER
4. TITLE (and Subtitle) (6) Rapid Solidification Processing, An Outlook (9)	5. TYPE OF REPORT & PERIOD COVERED Technical Report, no. 7, October 1978 to Jan. 1980
	6. PERFORMING ORG. REPORT NUMBER
7. AUTHOR(s) (10) M. Cohen (MIT), B. H. Kear (GTRC), and R. Mehrabian (NBS)	8. CONTRACT OR GRANT NUMBER(s) N00014-76-C-0071, NR031-795
9. PERFORMING ORGANIZATION NAME AND ADDRESS Massachusetts Institute of Technology, Cambridge, MA 02139	10. PROGRAM ELEMENT, PROJECT, TASK AREA & WORK UNIT NUMBERS (11) 11 Aug 80
11. CONTROLLING OFFICE NAME AND ADDRESS Office of Naval Research Arlington, VA 22217 (12) 25	12. REPORT DATE 11 August 1980
	13. NUMBER OF PAGES 17
14. MONITORING AGENCY NAME & ADDRESS (if different from Controlling Office) (13) N00014-76-C-0071, N00014-78-C-0387	15. SECURITY CLASS. (of this report) Unclassified
	15a. DECLASSIFICATION/DOWNGRADING SCHEDULE

16. DISTRIBUTION STATEMENT (of this Report)

This document has been approved for public release and sale; its distribution is unlimited

DTIC ELECTE AUG 28 1980 S D C

17. DISTRIBUTION STATEMENT (of the abstract entered in Block 20, if different from Report)

18. SUPPLEMENTARY NOTES

To be published in Proceedings of the 2nd Conference on Rapid Solidification Processing-Principles and Technologies, Reston, VA, 23-26 March 1980.

19. KEY WORDS (Continue on reverse side if necessary and identify by block number)

Rapid solidification, materials processing, atomization, consolidation, dendritic structures, segregate spacings, solute trapping, segregationless solidification, critical and hypercritical undercooling, grain refinement, microcrystallinity.

20. ABSTRACT (Continue on reverse side if necessary and identify by block number)

The elements of rapid solidification processing (RSP) are highlighted from the standpoints of (a) the fundamentals involved, (b) the prospects for new structure/property relationships, and (c) the interplay between materials processing and the wider field of materials science and engineering. Prototype methods of rapid solidification and consolidation are briefly described. Particular attention is then given to various solidification modes and resulting morphologies as a function of cooling rate from the molten state. These modes

DD FORM 1 JAN 73 1473 · EDITION OF 1 NOV 65 IS OBSOLETE S/N 0102-LF-014-6601

220000 all

SECURITY CLASSIFICATION OF THIS PAGE (When Data Entered)

AD A088473

DDC FILE COPY

80 8 28 045

span the range of planar, cellular, dendritic, and segregationless (microcrystalline) solidification, the latter being achieved by critical or hypercritical undercooling. The need for careful characterization of RSP microstructures is emphasized, and important scientific challenges for advancing the field of RSP are stressed.

Accession For
NTIS GRA&I
DDC TAB
Unannounced
Justification
By
Distribution/
Availability Codes
Dist | Avail and/or special
A

RAPID SOLIDIFICATION PROCESSING - AN OUTLOOK

M. Cohen
Massachusetts Institute of Technology, Cambridge, MA 02139
B. H. Kear
United Technologies Research Center, East Hartford, CT 06108
R. Mehrabian
National Bureau of Standards, Washington, D.C. 20234

ABSTRACT

Materials processing plays a central role in the general field of materials science and engineering; indeed, the recent surge of R&D activity in rapid solidification processing (RSP) provides a further example of how the advent of a processing method can catalyze new ideas across the wide spectrum of materials structure, properties, and performance. The major attention in RSP thusfar has been directed toward achieving fast cooling rates from the pre-alloyed liquid state, in the expectation that cost-beneficial properties in final shapes of technological importance can be obtained. Such processes typically involve (a) the solidification of small droplets, followed by their subsequent consolidation via powder-metallurgy techniques into bulk pieces, or (b) the melt spinning of continuous or discontinuous lengths of thin ribbons, or (c) the in-situ melting and solidification of thin surface layers.

Lagging behind, however, is a more basic understanding of the essential phenomena at play in RSP: (a) mechanisms and kinetics of nucleation and growth during rapid solidification; (b) connections between rapid solidification modes and resulting structures; (c) characterization of RSP fine-scale structures; and (d) definitive structure/property relationships to disclose which elements of the RSP structure are actually contributing to the novel properties being observed.

If RSP is to fulfill its promise for advanced technological applications, it is crucial to establish a sound body of knowledge for connecting the associated improvements in properties and performance back to the underlying microstructures as well as how the microstructures are attained.

1. Introduction

In this opening paper, we shall be concerned primarily with rapidly solidified crystalline materials, in contrast to the extensive attention that has been devoted to amorphous solids at other conferences[1]. Even in the present context, however, we are interested in the amorphous state and its controlled decomposition as a possible route toward attaining unique crystalline structures, and ultimately, new combinations of properties.

The term "processing" in the title of the present conference conveys a technological thrust to the phenomena involved in rapid solidification; implicit in the phrase "rapid solidification processing", or RSP as we shall abbreviate it, is the expectation that RSP will lead to significant advances in engineering applications and societal benefits. Nevertheless, even to such practical ends, a scientific foundation aimed at understanding the basic phenomena at play in RSP is becoming crucial to realizing the limitations as well as the promise of this burgeoning field of technical activity.

In a general sense, the processing of materials occupies a central place in materials science and engineering. Indeed, the interplay of internal structure, external properties, and performance in service--all of which are distinctive features of materials science and engineering--could not be responsive to the needs of society without the processing operations that make it feasible to produce, fabricate, and control materials in cost-effective ways to serve their respective functions. These interrelationships in materials science and engineering are portrayed schematically in Fig. 1. Correspondingly, materials processing can be described as those combinations of operations which are intended to produce and shape materials, as well as to control their properties, so that they can perform effectively for societal use.

Melting-and-casting, often called solidification processing in modern times, is well-recognized as one of the historic kinds of materials processing, especially in the field of metallurgy. For present purposes, we shall now regard rapid solidification as a subset of solidification processing in which the cooling rate is greater than about 10^2 K/s.

2. Advent of Rapid Solidification Processing

What has triggered the relatively sudden surge of interest in RSP[2]? Ever since the pioneering work of Pol Duwez in 1960 on splat quenching from the molten state[3], new horizons in structure/property relationships became accessible to the materials community and, as this conference will demonstrate, many approaches to such frontiers are being actively explored.

But the prospect of novel microstructures and new structure/property relationships does not fully account for the current spotlight on rapid solidification. The critical event in this saga was the emergence of a process, a process that produces rapidly solidified materials (superalloys for jet-engine applications, in this case) on a sufficient scale and with suitable quality to excite a quantum jump in technological potential. Of course, we are referring here to the advent of the Pratt and Whitney centrifugal atomizing process[4] with forced-convective cooling of the molten droplets to obtain cooling rates on the order of $10^5 - 10^6$ K/s.* Although other atomizing processes had long existed for pro-

* Pratt and Whitney has designated this process as RSR, standing for rapid solidification rate.

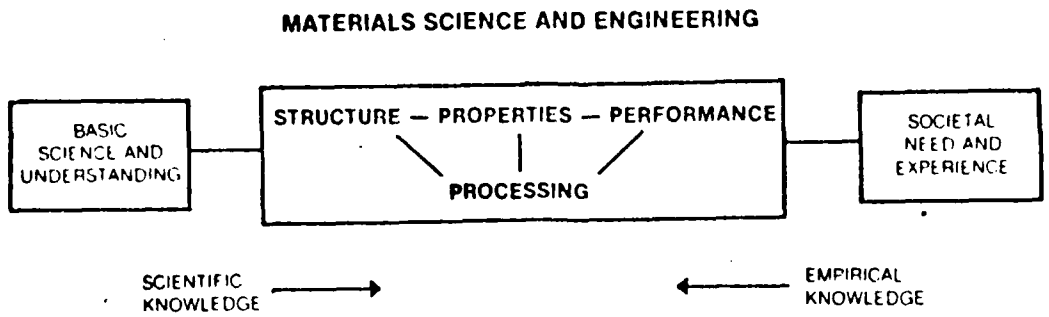

Fig. 1. A schematic representation of materials science and engineering.

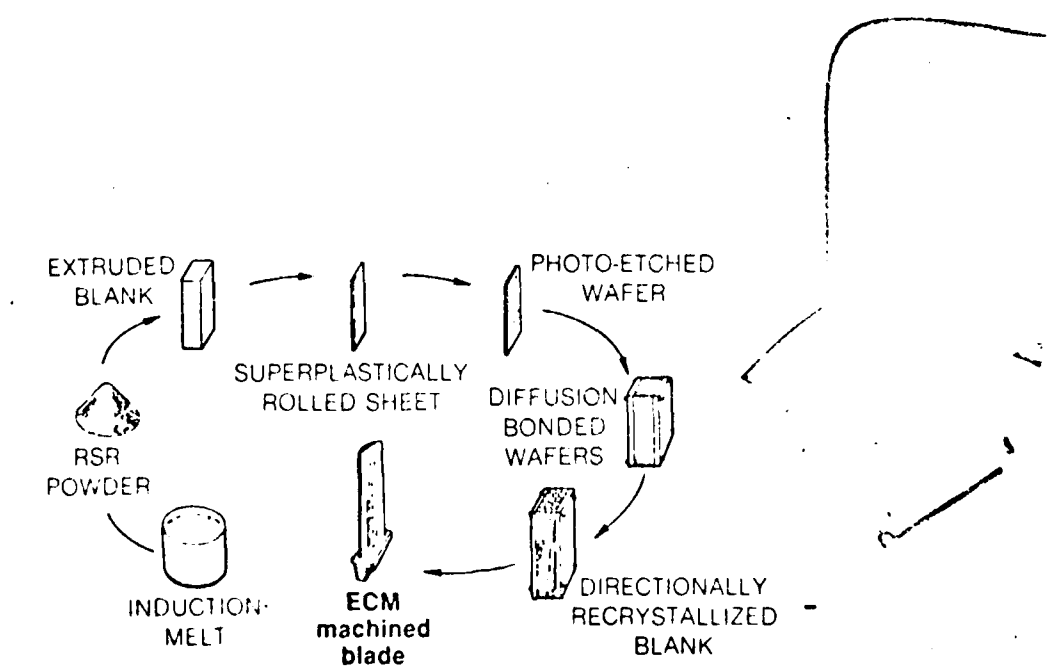

Fig. 2. Sequence of steps in the fabrication of a wafer blade.

ducing alloy powders (e.g., gas atomizing), and although faster cooling rates had been achieved by other methods (e.g., splatting), it was the timely Pratt and Whitney innovation that "brought the act together", even including a realistic method for consolidating the rapidly solidified powders into complex near-final shapes. All this caused the highly coupled materials-information-transfer system in Fig. 1 to "resonate", with empirical knowledge embodying the needs and experience of society flowing from right to left, while being met countercurrently by scientific knowledge and curiosity flowing from left to right. The resulting reverberation of ideas and motivations in the domain of RSP has given us a model example of how materials science and engineering operates in its interdisciplinary mode. Moreover, like so many other instances of materials innovation, the impetus of RSP seems to have originated more from societal pull than from scientific push. Yet we can be sure that, in the long run, the challenging promise of RSP will not be fully realized without the incisive explanations and refinements offered by the underlying science.

Already there is a remarkable pay-off in sight for RSP gas-turbine blades. The wafer-blade design in Fig. 2 combines the use of a new nickel-base alloy composition (6.8Al-14.5Mo-6.2W-0.06C) together with a complex array of built-in cooling channels, and thus allows about a 50 percent increase in the thrust-to-weight ratio over the current nickel-base hollow-cast blades made of PWA1422 (9Cr-10Co-2Ti-5Al-12.5W-0.1C-2Hf-0.015B). The rapid solidification step makes it possible to achieve hot-rolling superplasticity for producing strip stock, from which the wafers can be subsequently slotted and assembled by diffusion-bonding. With conventional casting instead of rapid solidification, the massive intermetallic phases in the new high-temperature alloy would render it too brittle for fabrication and service. It may also be noted that the desired columnar grains for high-temperature performance are grown in the final wafer blades by directional recrystallization, in contrast to the present practice of growing columnar grains in cast blades by directional solidification.

3. Some Typical Rapid Solidification and Consolidation Processes

For illustrative purposes only, we shall briefly refer to four rapid solidification processes, as depicted in Fig. 3. Two of these methods (gas atomization and centrifugal atomization) generate powders from small droplets, and so require later consolidation for producing bulk shapes. The other two (melt spinning and self-quenching) obtain rapid solidification in thin-layer form essentially by one-dimensional heat extraction.

Table I compares the maximum cooling rates that can be achieved realistically in rapid solidification processes for aluminum, iron, and nickel. Such limitations depend on the maximum feasible heat-transfer coefficients (second column) and the minimum practicable size dimensions (third column). The corresponding cooling rates in Table I range from 10^6 K/s for melt spinning to 10^8 K/s for thin-layer self-quenching. Clearly, then, these cooling rates are orders of magnitude faster than the modest 10^2 K/s which has been adopted to define the lower limit of "rapid solidification".

The most common methods of consolidation of RSP powders are hot isostatic pressing and hot extrusion (Fig. 4). Superplasticity may be involved in some cases and, if so, it permits the isothermal forging of extruded billets into near-final shapes. Of course, the latter feature is also embodied in hot isostatic pressing.

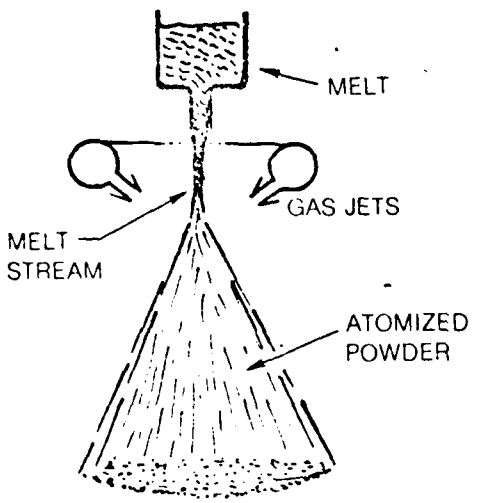

• INERT GAS ATOMIZATION

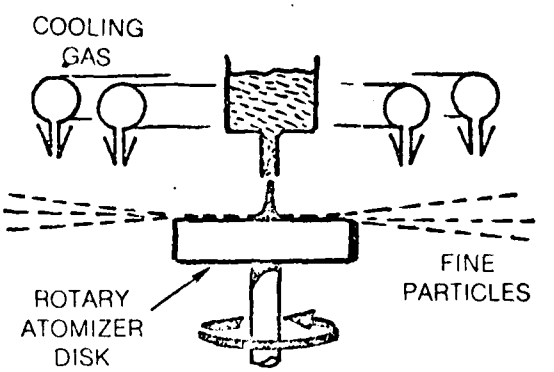

• CENTRIFUGAL ATOMIZATION

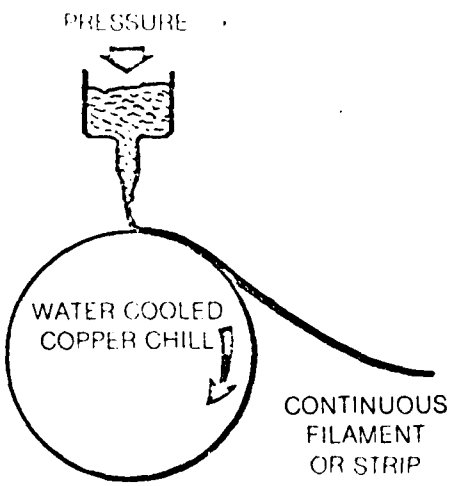

• MELT SPINNING

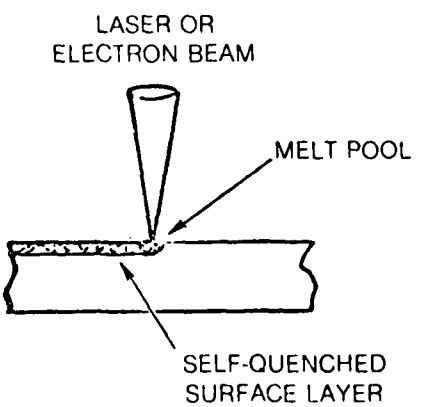

• SELF-QUENCHING

Fig. 3. Four typical methods of rapid solidification processing.

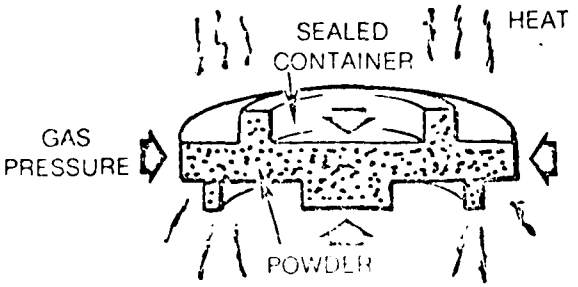

• HOT ISOSTATIC PRESSING

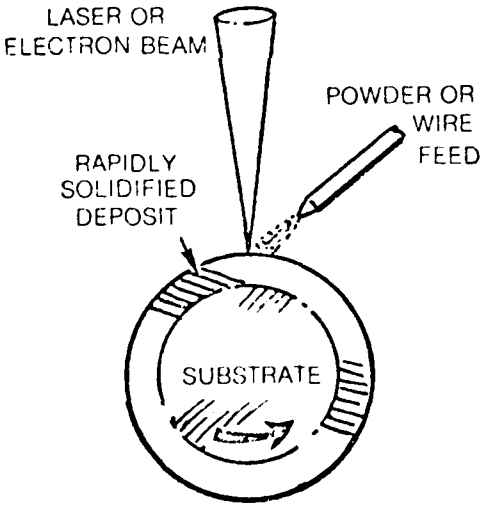

• INCREMENTAL SOLIDIFICATION

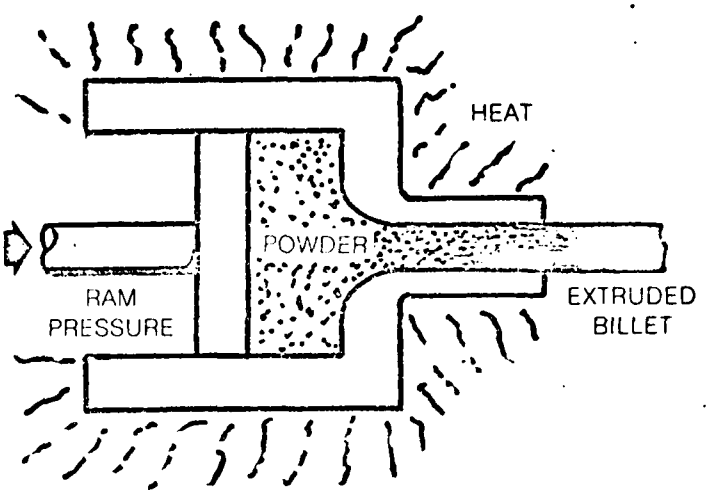

• HOT EXTRUSION

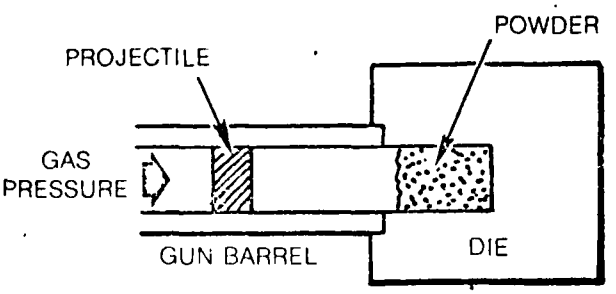

• DYNAMIC COMPACTION

Fig. 4. Four consolidation methods related to rapid solidification processing.

Incremental solidification in Fig. 4 (otherwise called layerglazing) provides a way of building up a three-dimensional shape by means of rapidly solidified layers; here, the rapid solidification and consolidation are carried out concurrently. This process is in the development stage[5], as is the indicated method of dynamic compaction[6]. The latter offers the interesting possibility of accomplishing rapid densification without requiring the high-temperature exposure associated with hot-forming operations. Hence, by using dynamic compaction, one can then study the effects of thermal treatments on bulk specimens of rapidly solidified materials subsequently to, and separately from, the consolidation step.

Whatever the method of consolidation, however, this aspect of RSP deserves greater attention because the structure/property relationships stemming from rapid solidification will obviously depend on the efficacy of the consolidation process as well as on the final heat treatment.

4. Microstructural Manifestations of Rapid Solidification

The microstructural consequences of rapid cooling from the molten state are summarized in Fig. 5. In passing from ordinary casting practice to cooling rates greater than 10^2 K/s, the microstructural features (including the scale of the microsegregation) become refined because the time for coarsening during solidification is reduced. This is why, for example, the dendritic arm spacings decrease with increasing cooling rate during solidification[7,8].. Nevertheless, for both the conventional and refined microstructures, conditions of local equilibrium (although not diffusional equilibrium) are considered to prevail at the solid/liquid interfaces, i.e., the local temperatures and coexisting compositions are given substantially by the equilibrium phase diagram. This means that the microstructural refinement in question results from differences in the growth process rather than from undercooling at the nucleation stage.

With still higher cooling rates, however, nucleation can be depressed to temperatures well below the liquidus temperature, and then novel microstructures come into existence. These are indicated in Fig. 5 as extended solid solutions, microcrystalline structures, metastable crystalline phases, and amorphous solids. In this regime, there can be large departures from local equilibrium at the advancing solid/liquid interfaces, with the solid-phase entrapping supersaturated concentrations of solute and impurity atoms such that, in the limit, the solid may have exactly the same (segregationless) composition as the parent liquid. We shall return to these nonequilibrium types of solidification later, but first it is desirable to deal in more detail with cases of local equilibrium at moving solid/liquid interfaces.

It should be emphasized that the three categories of microstructures blocked out in Fig. 5 must be regarded as very approximate; as indicated in this diagram, they will depend not only on the cooling rate, but also on compositional and process variables.

5. Interplay of Temperature Gradient and Solidification Rate Under Conditions of Local Interfacial Equilibrium

Three solidification-front morphologies are shown in Fig. 6 as controlled by the temperature gradient (G) in the liquid phase just ahead of the advancing interface and by the interface velocity or solidification rate (R), with local equilibrium being maintained at the interface. In these solidification processes, a steep temperature gradient tends to stabilize plane-front growth, whereas a

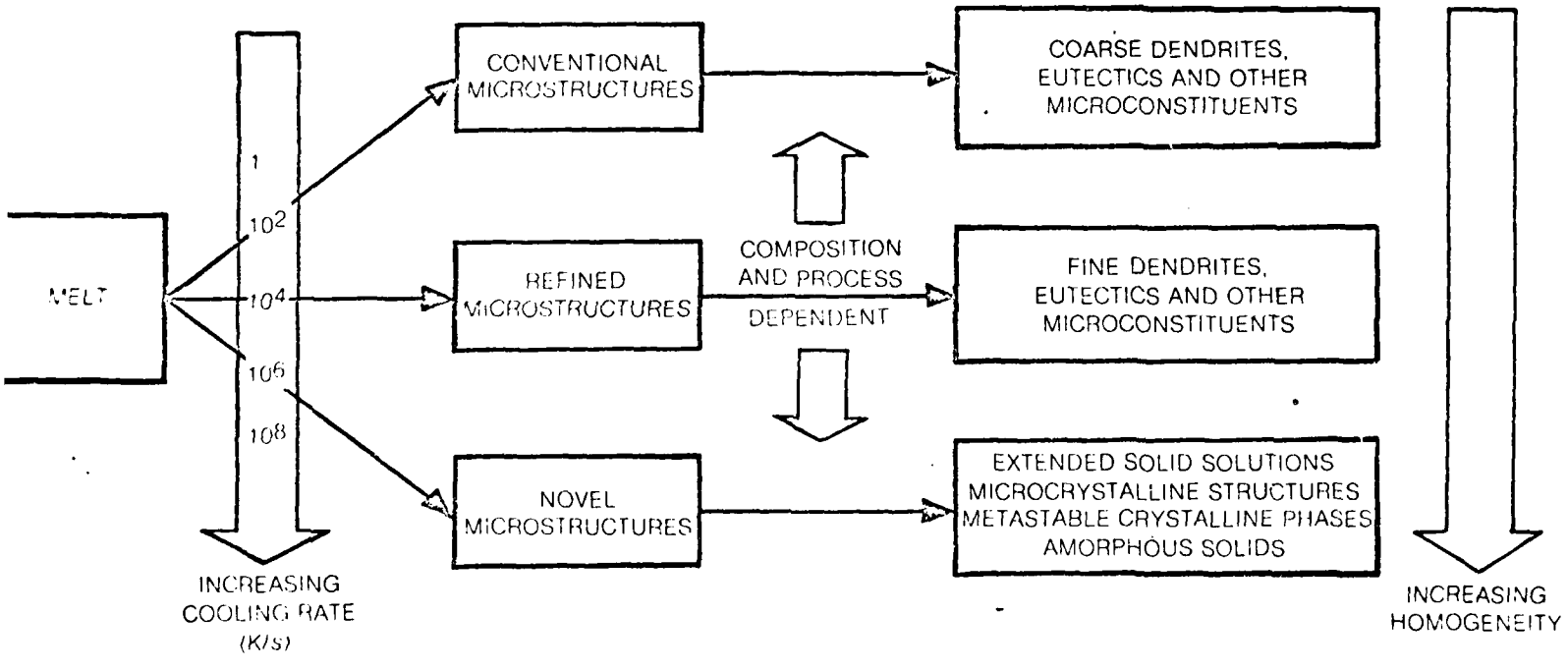

Fig. 5. Microstructural consequences of rapid solidification.
Note: these classifications are very approximate and depend on compositional and process variables as well as on the cooling rate.

FIRST LINE OF TEXT

FIRMLY MOUNT ALL PICTURES IN PROPER PLACE
TYPE FIGURES AND CAPTIONS IN THEIR RESPECTIVE SPACES TO ACCOMPANY ILLUSTRATIVE MATERIAL

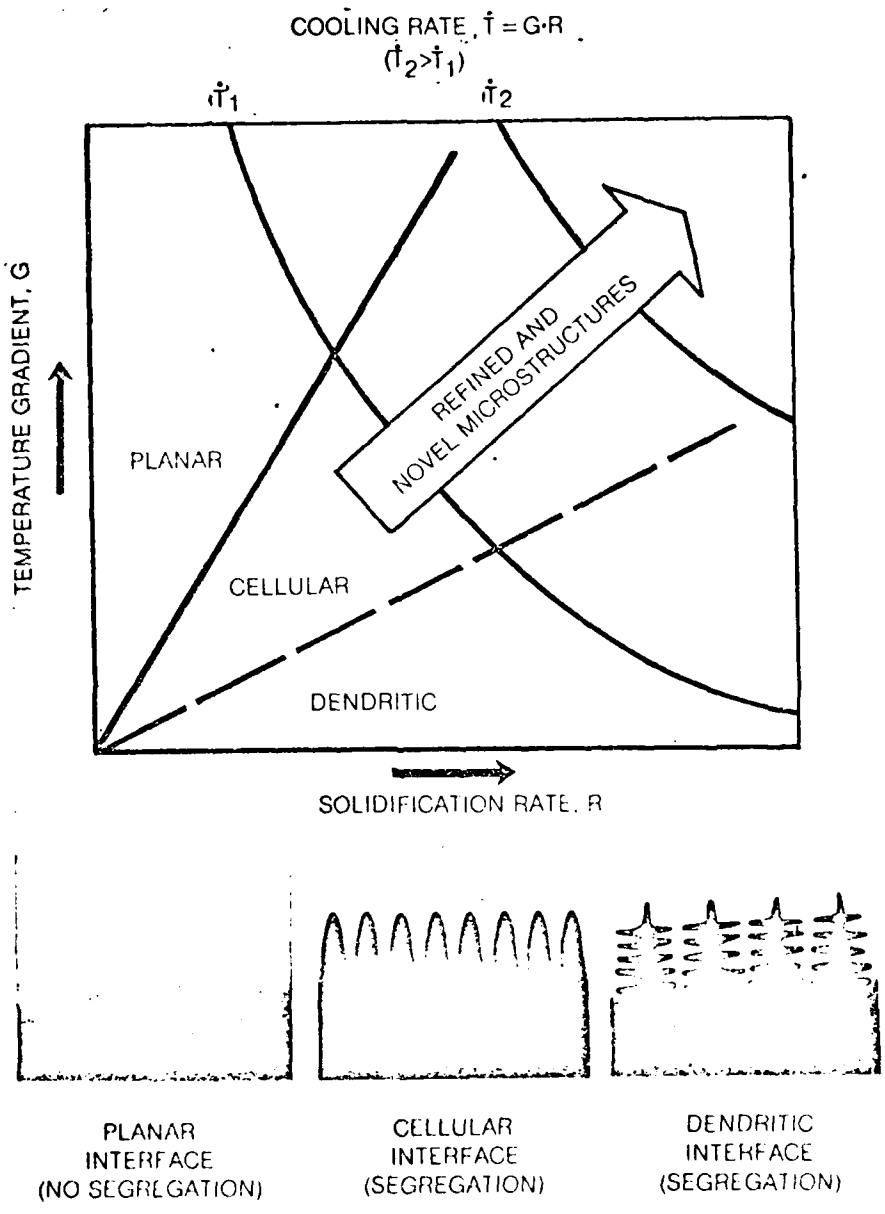

Fig. 6. Dependence of solidification morphology on temperature gradient (G) and solidification rate (R). The qualitative effect of increasing cooling rate ($\dot{T} = G.R$) is indicated by the sloping arrow.

steepness of the gradient (caused by equilibrium partitioning of the solute and solvent atoms) tends to destabilize a plane front. The boundary between the planar and cellular regions in Fig. 6 is the locus of G,R combinations that just balance the aforementioned two tendencies. To the left of (or above) this line, the temperature-gradient effect dominates, and plane-front growth is morphologically stable (with compositional homogeneity), whereas to the right of (or below) this line, the solute-gradient effect dominates and chance protuberances on an otherwise planar front become more and more pronounced (leading to microsegregations). The latter G,R combinations fall in the regime of constitutional undercooling[9], and result in cellular growth. With still larger solute gradients, due to faster solidification rates (R) relative to the operative temperature gradient (G), the familiar dendritic-growth morphology is encountered.

In the G,R space of Fig. 6, the product G.R is a measure of the cooling rate (T). Therefore, as indicated by the sloping arrow, moving out to larger G.R products in Fig. 6 corresponds to the microstructural changes caused by increasing cooling rates in Fig. 5.

An example of the microstructural refinement observed in aluminum alloys as a function of increasing cooling rate is given in Fig. 7. Although not shown explicitly, the G and R values at play here correspond to the dendritic regime in Fig. 6, and the segregate spacings plotted in Fig. 7 are determined by the dendritic arm spacings. Typical cooling-rate ranges, characteristic of various solidification methods, are also represented in Fig. 7. The reduction in segregate spacing by two orders of magnitude due to very rapid cooling is particularly significant from the standpoint of reaching compositional uniformity by homogenization treatments. Fig. 8 illustrates the remarkable reduction in diffusion time at 1600K required to reach 99 percent homogenization of tungsten in nickel for two segregate spacings typical of conventional solidification and for two segregate spacings typical of rapid solidification.

In discussing the regime of plane-front stability in Fig. 6, the additional stabilizing effect of solid/liquid surface energy was justifiably ignored because its contribution is negligible under the conditions at play. However, it has been shown[10,11] that, at high growth rates (R) and with the growth or decay of a perturbation (according to the laws of heat flow and solute diffusion) taken into account the surface energy becomes very important compared to the destabilizing effect of the solute gradient. This result is illustrated in Fig. 9, wherein it is seen that morphological stability can be attained if the interface velocity is sufficiently fast. Furthermore, this limiting velocity becomes insensitive to the temperature gradient. Thus, the G,R combinations of morphological stability (or homogeneous plane-front growth) are not confined simply to the avoidance of constitutional undercooling, as introduced schematically in Fig. 6, but actually extend around a dome-shaped region in Fig. 9 as shown by actual calculations for a Al-.1%Cu alloy[12]. The G,R combinations lying within the dome-shaped region lead to cellular or dendritic growth along with the associated compositional partitioning. The designated boundary of morphological stability falls inside the line of constitutional undercooling on the left and inside the line of surface-energy control (labeled absolute stability) on the right. It must not be expected, however, that the calculated right-hand limit will be valid if the interface velocity is so large that the boundary-layer thickness (liquid diffusivity divided by the growth rate) is reduced to only a few atomic jump distances.

FIRMLY MOUNT ALL PICTURES IN PROPER PLACE
TYPE FIGURES AND CAPTIONS IN THEIR RESPECTIVE SPACES TO ACCOMPANY ILLUSTRATIVE MATERIAL

FIRMLY MOUNT ALL PICTURES IN PROPER PLACE

TYPE FIGURES AND CAPTIONS IN THEIR RESPECTIVE SPACES TO ACCOMPANY ILLUSTRATIVE MATERIAL

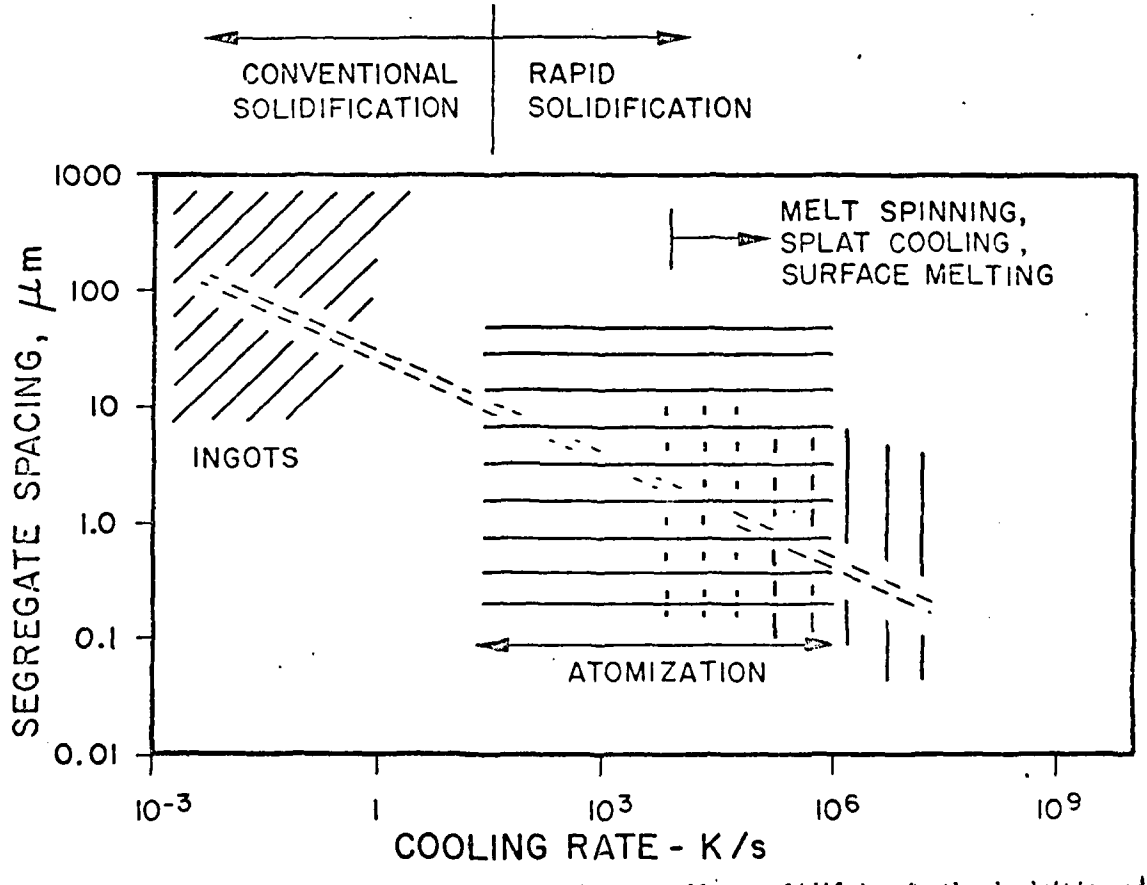

Fig. 7. Segregate spacing vs. cooling rate for aluminum alloys solidifying in the dendritic mode.

FIRST USE OF TEXT

FIRST LINE OF TEXT

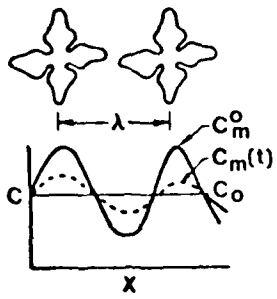

FIRST

$$\delta = \frac{C_{m(t)} - C_o}{C_m^o - C_o} = \text{microsegregation ratio}$$

- From Fick's Law

$$t = \frac{-\lambda^2 \ell n \delta}{4\pi^2 D}$$

$$= \frac{0.12\lambda^2}{D} \text{ for 99\% decay}$$

- For W in Ni

$$D_W^{Ni} = 2.08 \times 10^{-10} \text{ cm}^2/\text{sec at 1600 K}$$

$$t = 5.8 \times 10^8 \lambda^2 \text{ sec}$$

TYPICAL VALUES OF HOMOGENIZATION TIMES

	Conventional solidification		Rapid solidification	
λ(μm)	1000	100	10	1
t	10 weeks	16 hrs	10 mins	6 sec

Fig. 8. Effect of diffusion distance (λ) on the homogenization of a Ni-W alloy solidified at different cooling rates in the dendritic mode.

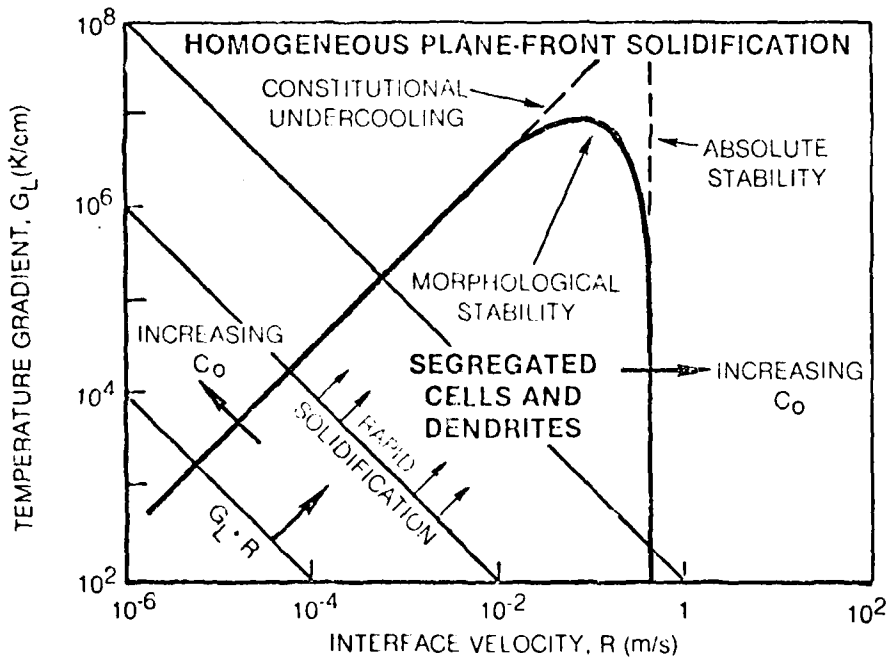

Fig. 9. Regimes of homogeneous plane-front growth vs. segregated cellular and dendritic growth as determined by the liquid temperature gradient (G_L) and the interface velocity (solidification rate, R) in Al-0.1% Cu. Dome-shaped line separating the two regimes is the locus of morphological stability (Ref. 12).

FIRMLY MOUNT ALL PICTURES IN PROPER PLACE
TYPE FIGURES AND CAPTIONS IN THEIR RESPECTIVE SPACES TO ACCOMPANY ILLUSTRATIVE MATERIAL

Each C.R line in Fig. 9 defines the locus of a given cooling rate, from which it is evident that the window on G,R combinations available for avoiding microsegregations becomes larger with increasing cooling rate. Conversely, this window becomes more restricted with increasing solute concentration (C_o).

6. Undercooling and Nonequilibrium Solidification

We now consider cases of solidification in which nucleation of the solid phase sets in at temperatures significantly below the liquidus temperature (T_L) of the alloy at hand (see Fig. 10). Such instances may come about because of very rapid cooling (beyond the rates discussed in Section 5) or because of some reduction in the potency of heterogeneous nucleation sites. To avoid unnecessary complications for present purposes, we shall assume adiabatic conditions, i.e., the latent heat of solidification (ΔH) is absorbed fast enough within the system so that, effectively, any heat removal from the system during solidification is inconsequential.

Critical undercooling is indicated as Case 2 in Fig. 10, wherein nucleation occurs at T_2 and the recalescence temperature (T_R) at the solid/liquid interface is raised barely to the solidus temperature (T_S). This means that

$$\Delta H = \int_{T_2}^{T_S} C_p^{\ell}\, dT,$$

and so solidification can take place massively--entirely within the single-phase α field and without compositional partitioning or local equilibrium at the interface. Case 1 exemplifies hypocooling; here, $T_1 > T_2$ and $T_R > T_S$. Thus, although the solidification starts in the massive mode, local equilibrium and compositional partitioning can ensue when the interfacial temperature rises into the α + liquid field. This kind of solidification sequence accounts for the solute-rich cores which have been noted in some dendritic structures[13]. Case 3, with $T_3 < T_2$ and $T_R < T_S$, illustrates hypercooling. Cases 2 and 3 both result in segregationless solidification (namely, complete solute trapping to produce a uniform composition in the solid equal to C_o), but because the nucleation rate is likely to be faster, and the growth rate slower, at the lower temperature, we can expect a smaller microcrystalline grain size if the solidification process can be depressed to the lower temperature. We shall come back to the subject of microcrystallinity later..

Another type of undercooling is represented in Fig. 11. Here, we imagine that the β phase is not able to nucleate. In other words, the extended liquidus and solidus lines denote the compositions of the liquid and α phases coexisting in metastable equilibrium below the eutectic temperature. If, in addition, the α solidification can be undercooled, then the previously described conditions of hypocooling, critical undercooling, and hypercooling are also possible in this case, even though the composition C_o may now be much more concentrated than the maximum α solid solubility limit given in Fig. 10.

Needless to say, undercooling may also result in the formation of new metastable phases, whether crystalline or amorphous. Such an example is illustrated in Fig. 12, which merely extends the rationale of Figs. 10 and 11. The conditions in the middle diagram have been chosen to indicate critical undercooling of the metastable γ phase, with suppression of the more stable mixture of α and β phases. In the right-hand diagram, even the γ phase is suppressed and the liquid is undercooled to below the glass-transition temperature (T_g) where the metastable amorphous state is formed; this is a special case of hypercooling in which $\Delta H = 0$.

FIRST LINE OF TITLE
AUTHOR'S NAMES
AUTHOR'S AFFILIATIONS
FIRMLY MOUNT ALL PICTURES IN PROPER PLACE
TYPE FIGURES AND CAPTIONS IN THEIR RESPECTIVE SPACES TO ACCOMPANY ILLUSTRATIVE MATERIAL

FIRMLY MOUNT ALL PICTURES IN PROPER PLACE

TYPE FIGURES AND CAPTIONS IN THEIR RESPECTIVE SPACES TO ACCOMPANY ILLUSTRATIVE MATERIAL

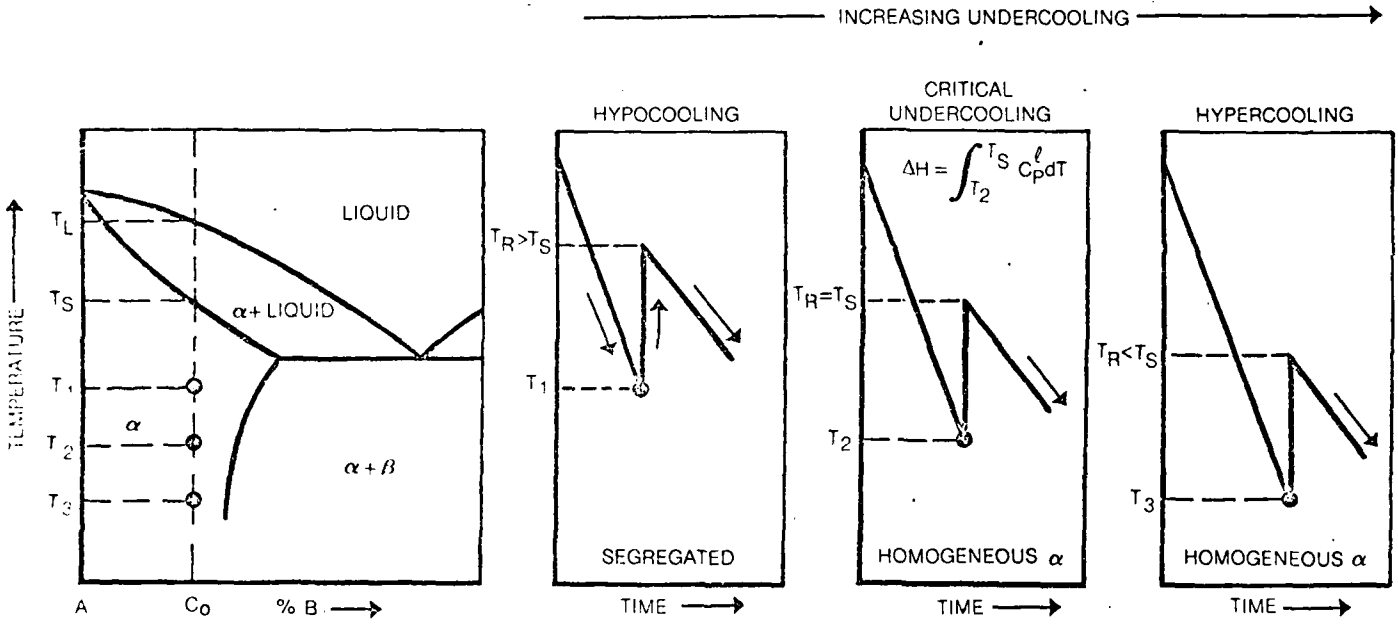

Fig. 10. Illustration of hypocooling, critical undercooling, and hypercooling for adiabatic solidification of the α phase. T_1, T_2 and T_3 are the respective undercooling temperatures; T_R designates the recalescence temperature in each case.

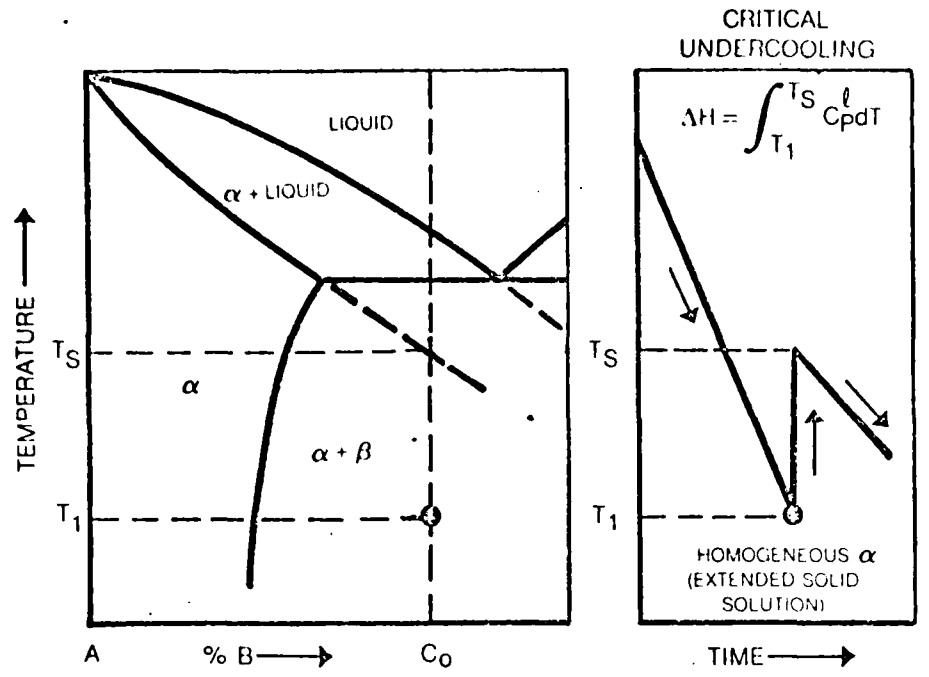

Fig. 11. Illustration of critical undercooling for adiabatic solidification of the α phase with extended (metastable) solubility.

ABSTRACT

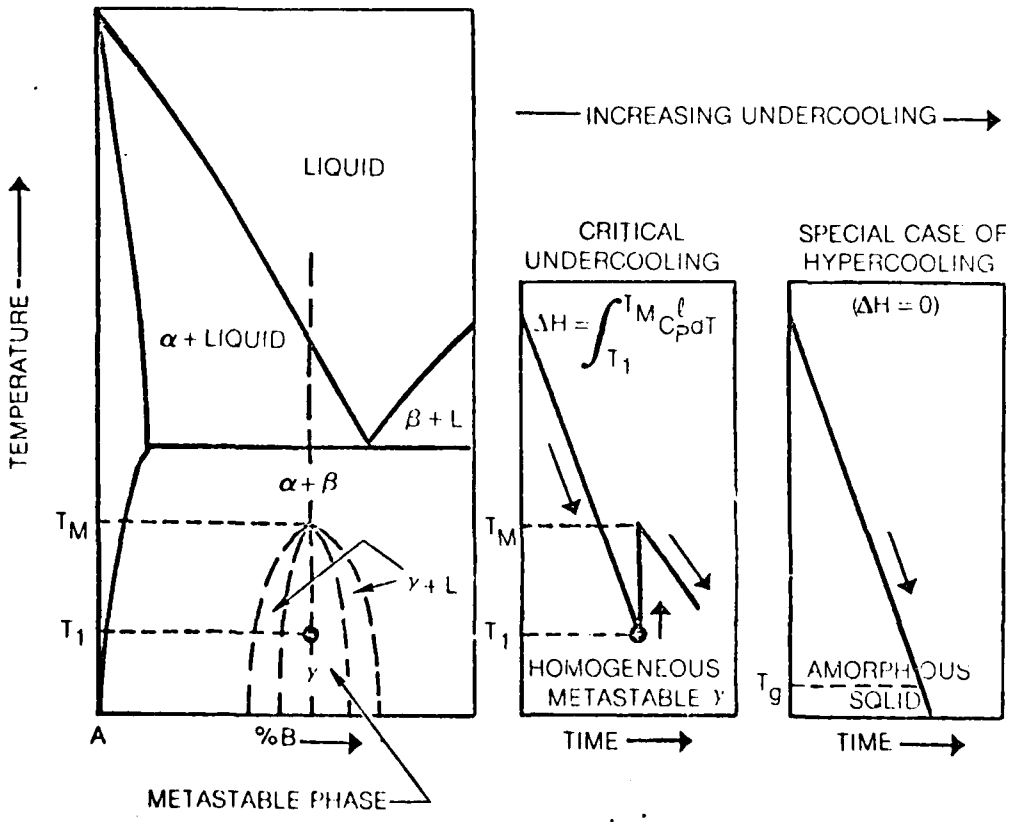

Fig. 12. Illustration of critical undercooling and hypercooling for adiabatic solidification of a metastable γ phase. T_M is the melting point of the γ phase. Formation of an amorphous phase is shown as a special case of hypercooling with $\Delta H = 0$.

FIRMLY MOUNT ALL PICTURES IN PROPER PLACE
TYPE FIGURES AND CAPTIONS IN THEIR RESPECTIVE SPACES TO ACCOMPANY ILLUSTRATIVE MATERIAL

It is worth re-emphasizing that heterogeneous nucleation sites play a vital role in determining whether or not hypercooling or novel microstructures can be attained instead of, say, refined dendritic microstructures. A transition range between these two modes of solidification is shown schematically in Fig. 13[14]. The cooling rate required to avoid dendritic solidification (hence, to achieve massive solidification) becomes less drastic with decreasing number and potency of the heterogeneous nucleation sites. Indeed, with small-droplet dispersions or emulsions[15] which thereby isolate the extraneous nucleants among some of the droplets, the remaining "clean" droplets may be readily hypercooled even on relatively slow cooling from the liquid state. Clearly, then, such variations as melt cleanliness and melt superheating may become determining factors in whether massive solidification will be reached or not.

7. Massive Solidification and Microcrystallinity

The massive solidification that takes place on hypercooling not only yields grains of uniform composition, but is also capable of producing an extremely small as-solidified grain size--in the range of 1 μm or less, hence, the term microcrystalline. Moreover, unlike cells or dendritic arms, adjacent microcrystallites tend to have large-angle boundaries because they originate from independent nucleation events.

Calculations have been carried out[16] for the nucleation rate (I) and growth rate (R) in Al solidification during fast cooling (10^6 - 10^8 K/s), taking the evolved heat of solidification into account. Although fraught with many uncertainties because of the assumptions and estimates introduced, the calculated cooling curves in Fig. 14 indicate that the undercooling increases with the cooling rate and, because of recalescence, the solidification in each instance completes itself over a relatively narrow temperature range. If, therefore, the nucleation and growth rates are assumed to be constant during the respective solidification runs, the resulting grain size can be expressed as $\bar{d} = (R/I)^{\frac{1}{4}}$, and is plotted in Fig. 15 as a function of cooling rate. These calculations are in approximate agreement with the observed grain sizes in splatted foils of Al. However, this may be fortuitous in view of the way that the critical free energy of nucleation (or the solid-liquid interfacial energy) and the temperature dependence of liquid viscosity (or diffusivity) were estimated for these calculations[16]. Better approximations of the nucleation parameters should now be possible considering the larger-than-usual undercoolings found more recently by using the small-droplet technique to diminish the interference of heterogeneous nucleation[17].

Another route for obtaining microcrystallinity is through crystallization of the amorphous state[18,19]. For example, on heating an Fe-B glass, the bcc Fe phase (supersaturated with B) which forms has an extremely-small particle size of about 0.05 μm; but the alloy becomes quite brittle at this stage.

8. Characterization of Rapidly Solidified Microstructures

To delineate and quantify the fine-scale microstructural features of rapidly solidified alloys remains a central problem in the field of RSP. Such characterization would include the quantitative electron microscopy and microdiffraction of cells, dendrites, microcrystallites, and dispersed phases, together with compositional profiles and interfacial misorientations. The importance of this microstructural approach is generally two-fold: (a) it sheds light on the mode of solidification and the operational factors that have generated the structure being examined, and (b) it provides a scientific basis for the structure/property

FIRMLY MOUNT ALL PICTURES IN PROPER PLACE
TYPE FIGURES AND CAPTIONS IN THEIR RESPECTIVE SPACES TO ACCOMPANY ILLUSTRATIVE MATERIAL

FIRMLY MOUNT ALL PICTURES IN PROPER PLACE
TYPE FIGURES AND CAPTIONS IN THEIR RESPECTIVE SPACES TO ACCOMPANY ILLUSTRATIVE MATERIAL

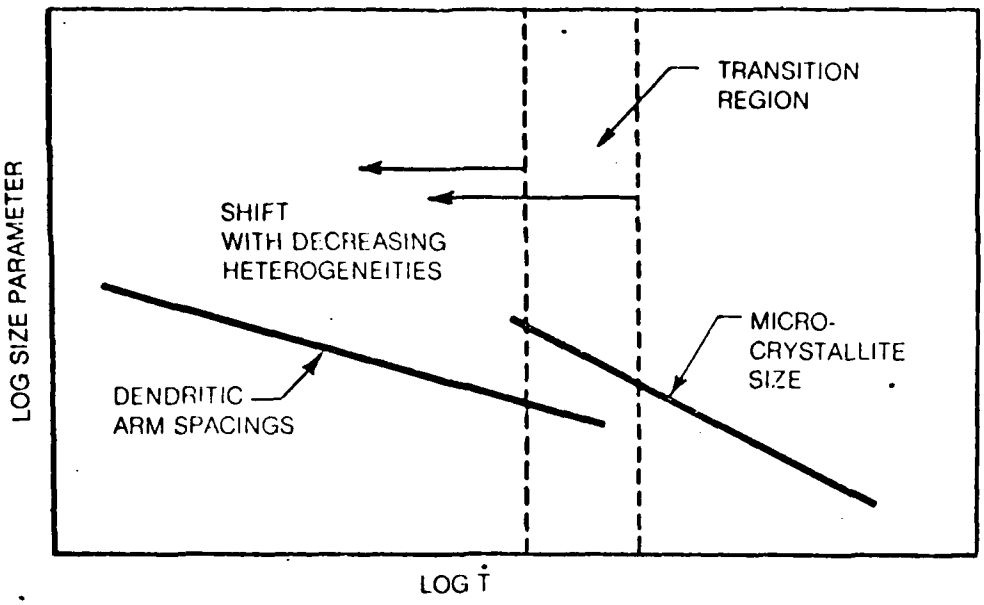

Fig. 13. Effect of cooling rate on dendritic arm spacing and microcrystalline grain size; the transition region is shifted to lower cooling rates with reduction in the efficacy of heterogeneous nucleation[14].

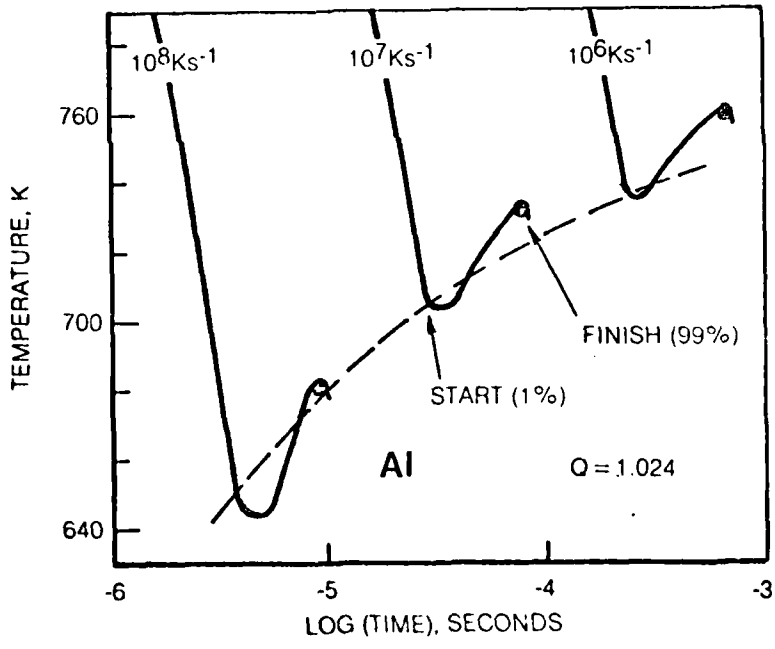

Fig. 14. Calculated cooling curves for the hypercooled solidification of Al at three high cooling rates; showing recalescence due to the latent heat of solidification. The Q parameter is obtained from an assumed critical free energy of nucleation at a selected degree of undercooling[16].

FIRST LINE

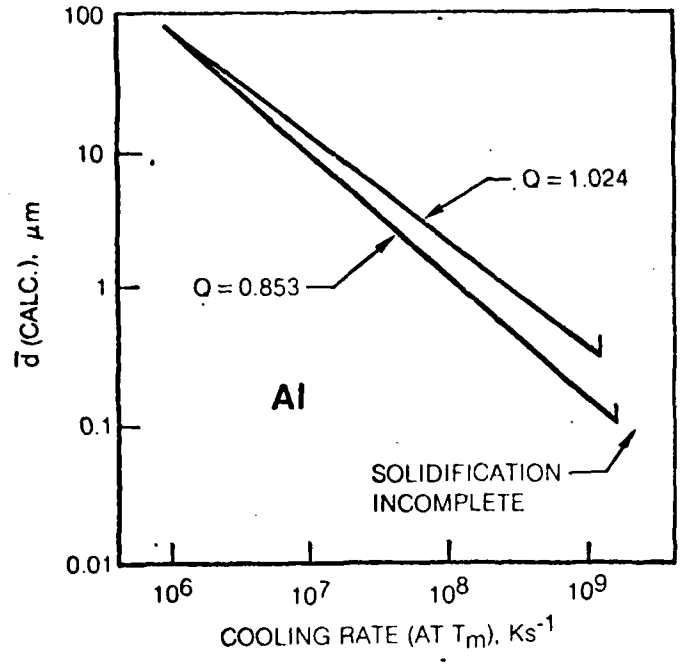

Fig. 15. Calculated grain size of as-solidified Al based on cooling curves in Fig. 14 (labeled Q = 1.024). Better agreement with the observed minimum grain size in splat-quenched Al foils is obtained by adjustment of Q to 0.853. The calculations show a minimum grain size cut-off (at 0.4 to 0.1 μm for the two Q values, respectively) because of the C-curve dependence of the nucleation rate on temperature (16).

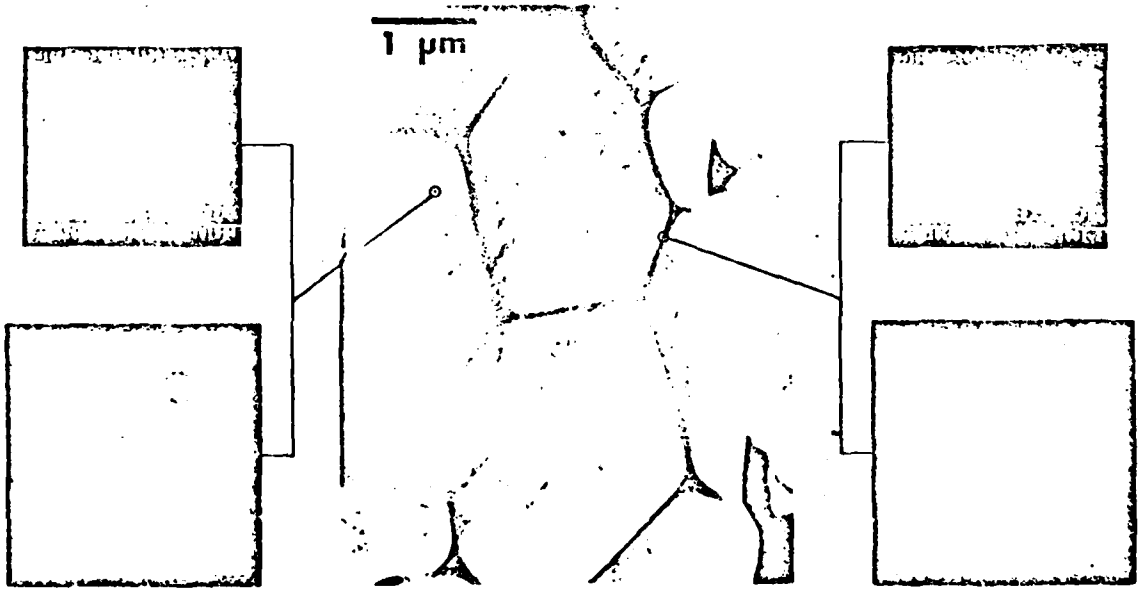

Fig. 16. Microstructural examination of high-phosphorus austenitic steel RSP powder. Center - STEM bright-field image showing cellular structure, with second phase at cell boundaries. Lower left and right - microdiffraction patterns from indicated points; cell-boundary phase is amorphous. Upper left and right - electron energy-loss spectra, indicating no carbon build-up at cell boundary(20).

FIRST LINE
FIRMLY MOUNT ALL PICTURES IN PROPER PLACE
TYPE FIGURES AND CAPTIONS IN THEIR RESPECTIVE SPACES TO ACCOMPANY ILLUSTRATIVE MATERIAL

relationships which may emerge from RSP. As it happens, this link in the knowledge-transfer system of Fig. 1 is presently quite weak!

We shall mention here only two microstructural studies reported in these Proceedings. The STEM bright-field image[20] in Fig. 16 (center) shows the cellular structure of a high-phosphorous austenitic steel after rapid solidification (centrifugal atomizing and convective cooling). Surprisingly, the phase along the cell boundaries turns out to be amorphous, in contrast to the expected crystalline structure of the cells themselves (cf. microdiffraction patterns in the lower left and right of Fig. 16). The crystalline patterns contain Kikuchi lines and these disclose very little misorientation between adjacent cells. According to the electron energy-loss spectra (upper left and right), there has been no detectable carbon build-up at the cell boundaries. On the other hand, the microchemical profiles, as determined by X-ray fluorescence spectra with the STEM and plotted in Fig. 17, reveal appreciable boundary segregation of P, Cr, and Ni. Undoubtedly, the phosphorus concentration together with the rapid cooling will account for retaining the amorphous phase. It is evident that compositional uniformity, as would be realized from massive solidification, was not achieved under the cooling conditions at play.

On a different scale, Fig. 18 shows the austenitic grain-growth characteristics of rapidly solidified and extrusion-consolidated 9Ni-4Co steels, in comparison with the same steels conventionally processed[21]. The RSP material exhibits remarkable resistance to grain growth, even up to 1200°C. The indications are that this inhibited grain growth is probably caused by an extremely fine dispersion of MnS particles resulting from the rapid solidification step. Indeed, one of the noteworthy benefits of RSP may turn out to lie in the distribution control of relatively insoluble microconstituents. There are obvious implications here from the standpoint of mechanical properties that may now be reached in ultrahigh-strength steels.

9. Scientific Challenges

We conclude with a brief list of scientific challenges in the field of RSP, which arise either explicitly or implicitly from the foregoing text:

A. A still-deeper understanding is needed of nucleation, growth, segregation, and phase sequences under conditions of rapid cooling and various degrees of undercooling.

B. New approaches for mapping metastable phase fields are desired.

C. Experimental methods for measuring thermal fields during rapid solidification have to be developed and applied, in conjunction with more realistic heat-flow models.

D. Quantitative characterization of the fine-scale microstructures associated with rapid cooling and undercooling is now essential. Special effort should be given to microcrystalline structures.

E. Using the amorphous state as precursor to forming novel crystalline structures requires detailed attention.

FIRMLY MOUNT ALL PICTURES IN PROPER PLACE
TYPE FIGURES AND CAPTIONS IN THEIR RESPECTIVE SPACES TO ACCOMPANY ILLUSTRATIVE MATERIAL

AUTHOR NAME
AUTHOR'S AFFILIATIONS

THIS PAGE IS BEST QUALITY PRACTICABLE
FROM COPY FURNISHED TO DDC

FIRST LINE OF TEXT

FIRST LINE OF TITLE

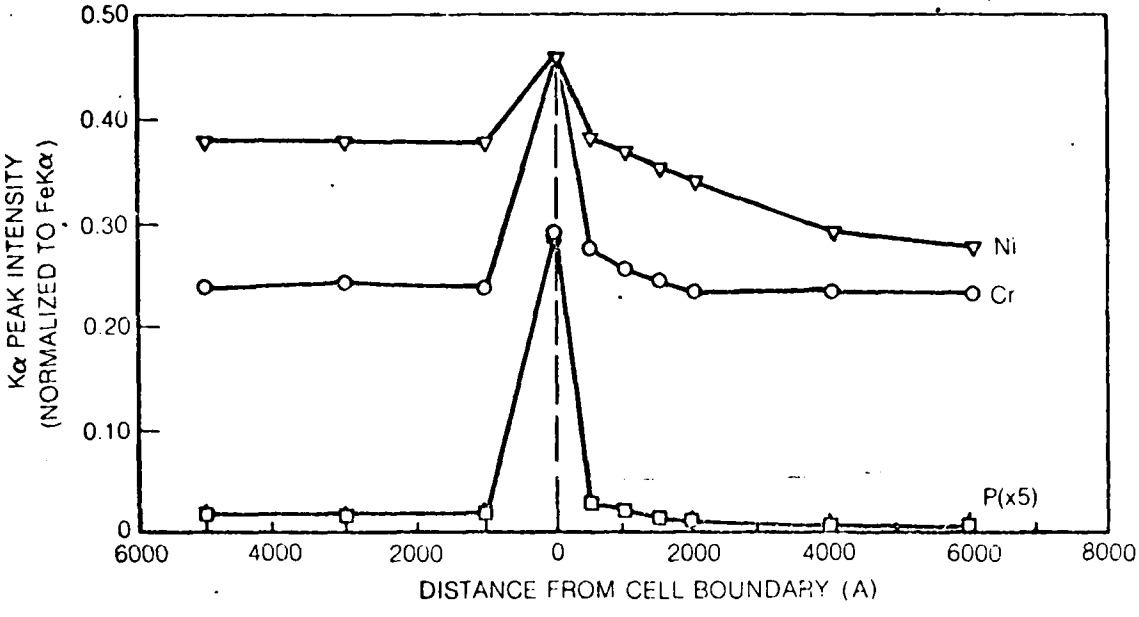

Fig. 17. Microchemical profiles across two adjacent crystalline cells and the intervening amorphous boundary phase in high-phosphorus austenistic RSP powder[20].

FIRMLY MOUNT ALL PICTURES IN PROPER PLACE
TYPE FIGURES AND CAPTIONS IN THEIR RESPECTIVE SPACES TO ACCOMPANY ILLUSTRATIVE MATERIAL

FIRST LINE OF TEXT

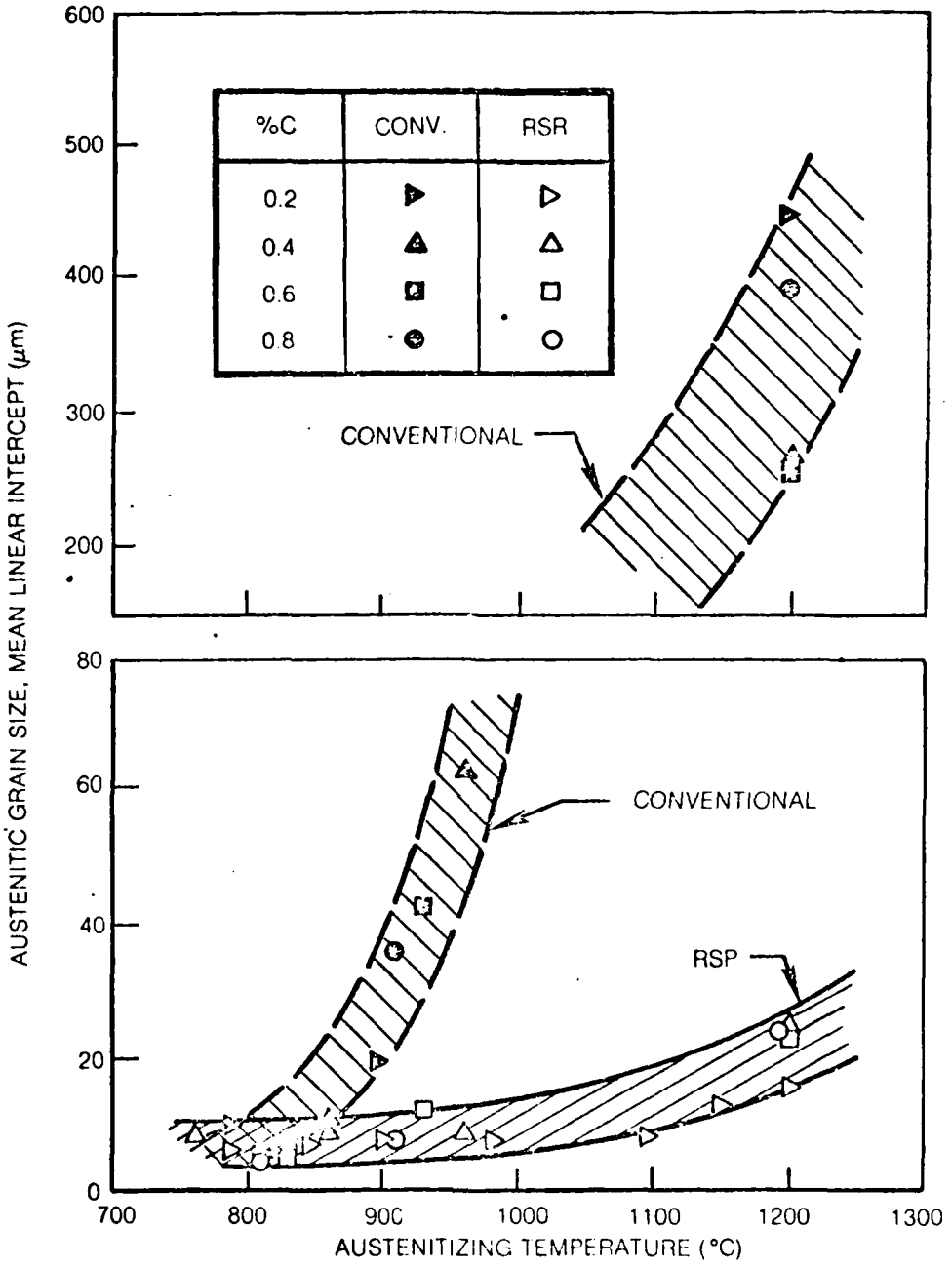

Fig. 18. Austenitic grain size of 9Ni-4Co steels vs. austenitizing temperature (1 hr.) comparing conventially processed and RSP steels[21].

FIRMLY MOUNT ALL PICTURES IN PROPER PLACE
TYPE FIGURES AND CAPTIONS IN THEIR RESPECTIVE SPACES TO ACCOMPANY ILLUSTRATIVE MATERIAL

FIRMLY MOUNT ALL PICTURES IN PROPER PLACE
TYPE FIGURES AND CAPTIONS IN THEIR RESPECTIVE SPACES TO ACCOMPANY ILLUSTRATIVE MATERIAL

DO NOT TYPE OVER THIS LINE

fundamentals of powder compaction and subsequent processing need particular study in the light of RSP and the microstructural changes involved.

G. Virtually untouched thusfar is a basic model-experiment approach to structure/property relationships in RSP materials. This part of the overall RSP program is likely to become a key element in determining just what aspects of RSP are actually responsible for improved performance and, in turn, just what goes on during rapid solidification and subsequent processing to generate the microstructural features which are really important.

All of these challenges are closely interrelated, and offer a timely example of materials science and engineering "at work".

AUTHORS' AFFILIATIONS

Acknowledgments

The authors are indebted to the following agencies for their research support in the field of rapid solidification processing: at MIT by the Office of Naval Research under Contract N00014-76-C-0171, NR031-795; at United Technologies by the Defense Advanced Research Projects Agency under Contract F33615-76-C-5136 and N00014-78-C-0387; and at the National Bureau of Standards by the Defense Advanced Projects Agency under Contract Order 3751. We would also like to express our appreciation to Mr. H. C. Brown for preparing the illustrative material in this paper.

Certain commercial equipment, instruments, or materials are identified in this paper in order to adequately specify the experimental procedure. In no case does such identification imply recommendation or endorsement by the National Bureau of Standards, nor does it imply that the material or equipment identified is necessarily the best available for the purpose.

TABLE I

COOLING RATE LIMITATIONS IN RSP

	HEAT TRANSFER COEFFICIENT	USEFUL LOWER SIZE LIMIT	AVG. MAX. COOLING RATE IN LIQUID Al, Fe, Ni
ATOMIZATION	$\sim 10^5 W/m^2 \cdot K$	$\sim 10 \mu m$	$\sim 1.5 \times 10^7 K/s$
MELT SPINNING	$\sim 10^5$	~ 25	$\sim 10^6$
SELF QUENCHING	TENDS TO INFINITY	~ 10	$\sim 10^8$

FIRST LINE OF TEXT

References

1. Proc. Second International Conference on Rapidly Quenched Metals, N. J. Grant and B. C. Giessen, Eds., Materials Science and Engineering, Vol. 23, 1976; and Proc. Third International Conference on Rapidly Quenched Metals, B. Cantor, Ed. , The Metals Society, Vols. I and II, 1978.

2. Proc. First International Conference on Rapid Solidification Processing: Principles and Technologies, R. Mehrabian, B. H. Kear, and M. Cohen, Eds., Claitor's Publishing Division, Baton Rouge, LA, 1977.

3. P. Duwez, R. H. Willens, and W. Klement, J. Applied Physics, Vol. 31, p. 1136, 1960; Trans. Met. Soc. AIME, Vol. 227, p. 362, 1963.

4. P. R. Holiday, A. R. Cox, and R. J. Patterson, Ref. 2, p. 246, 1977.

5. E. M. Breinan and B. H. Kear, Ref. 2, p. 87, 1977.

6. C. F. Cline, J. Mahler, M. Finger, W. Kuhl, and R. Hopper, Ref. 2, p. 380, 1977; and D. G. Morris, these Proceedings.

7. M. C. Flemings, Solidification Processing, McGraw-Hill, NY, p. 151, 1974.

8. R. Mehrabian, Ref. 2, p. 9, 1977.

9. M. C. Flemings, ibid, 58.

10. S. R. Coriell and R. F. Sekerka, these Proceedings.

11. J. W. Cahn, S. R. Coriell, and W. J. Boettinger, Symp. on Laser and Electron Beam Processing, C. W. White and P. S. Peercy, Eds., Materials Research Society, Boston, MA, Nov. 28, 1979.

12. S. R. Coriell (private communication); see also S. R. Coriell and R. F. Sekerka, these Proceedings.

13. R. Mehrabian, Ref. 2, p. 14, 1977.

14. J. P. Hirth, Met. Trans., Vol. 9A, p. 401, 1978.

15. J. H. Perepezko, D. H. Rasmussen, I. E. Anderson, and C. R. Loper, Proc. Sheffield International Conference on Solidification and Casting of Metals, The Metals Society, London, p. 169, 1979.

16. P. G. Boswell and G. A. Chadwick, Scripta Metl, Vol. 11, p. 459, 1977.

17. J. H. Perepezko, these Proceedings.

18. J. L. Walter, these Proceedings.

19. K. S. Tan, T. Wahl, and R. Kaplow, these Proceedings.

20. T. F. Kelly and J. B. Vander Sande, these Proceedings.

21. M. Suga, J. L. Goss, G. B. Olson, and J. B. Vander Sande, these Proceedings.

AUTHORS' NAMES

AUTHORS' AFFILIATIONS

ABSTRACT

FIRMLY MOUNT ALL PICTURES IN PROPER PLACE
TYPE FIGURES AND CAPTIONS IN THEIR RESPECTIVE SPACES TO ACCOMPANY ILLUSTRATIVE MATERIAL